

Seismic tests of precast concrete, moment-resisting frames and connections

Weichen Xue and Xinlei Yang

Precast concrete structures have fundamental advantages: increased speed of construction, improved quality control due to the member-fabrication environment, and reduced site formwork and labor.¹ Precast concrete structures are widely used in many countries, including the United States, New Zealand, and Japan.

Post-earthquake field investigations of precast concrete structures after the 1994 Northridge earthquake, the 1995 Kobe earthquake, and the 2008 Wenchuan earthquake in China showed that many precast concrete structures failed in those destructive earthquakes.^{2,3} It was therefore necessary to evaluate the seismic behavior of precast concrete frames used in high seismic zones. In the past decades, some experimental investigations have been conducted in the United States, New Zealand, Japan, and China to investigate the seismic behavior of precast concrete connections under cyclic loading.

Three full-scale exterior precast concrete beam-to-column connections were tested at the University of Canterbury in Christchurch, New Zealand,⁴ and it was reported that the specimens detailed for seismic loads performed satisfactorily in terms of strength, ductility, and energy dissipation and could be used in ductile moment-resisting frames. French et al.^{5,6} studied three different types of precast concrete connections and concluded that the energy dissipation and the strength of precast concrete connections were adequate with respect to monolithic concrete specimens. Englekirk developed an energy-absorbing, ductile connector that could be used to construct a seismic moment-resisting frame of precast concrete components that would outperform comparable cast-in-place systems.⁷

Editor's quick points

- This paper presents the results of experimental investigations on four full-scale precast concrete connections and a half-scale, two-story, two-bay precast concrete, moment-resisting frame.
- The precast concrete connections investigated in this paper included an exterior connection, an interior connection, a T connection, and a knee connection.
- Test results revealed that the four precast concrete connections exhibited a strong column–weak beam failure mechanism and failed due to concrete crushing and fracturing of longitudinal bars as a result of forming a plastic hinge at the fixed end of the beam.

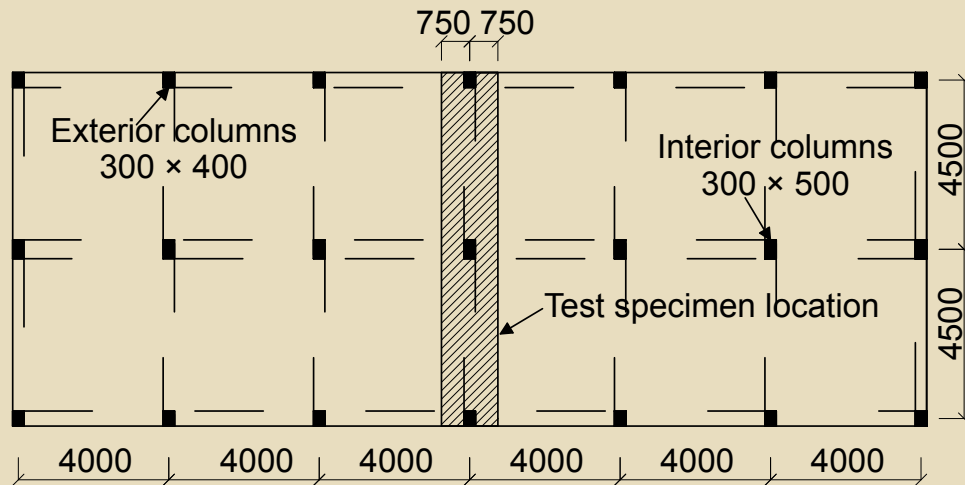


Figure 1. This diagram illustrates the structural-plan layout of the prototype frame building. Note: All dimensions are in millimeters. 1 mm = 0.0394 in.

Priestley et al.⁸ presented a paper about a test of two ungrouted, post-tensioned, precast concrete beam-to-column joint subassemblies under cyclic loading. They reported that satisfactory seismic performance could be expected from well-designed, ungrouted, precast, post-tensioned concrete frames. Ertas et al.⁹ studied four types of ductile moment-resisting precast concrete connections and one monolithic concrete connection, which were all designed for use in high seismic zones. Through comparisons of performance parameters such as energy dissipation and ease of fabrication, it was revealed that the modified bolted joint might be suitable for use in high seismic zones. In addition, researchers studied the behavior of precast concrete connections to find a suitable connecting method that would ensure the ductility and stiffness of precast concrete structures.^{10–12}

As for precast concrete frames, only a few experimental investigations have been conducted to examine the seismic behavior of precast concrete frames. Priestley et al.¹³ tested a five-story precast concrete frame and concluded that the seismic behavior of the test structure was satisfactory and the damage in the frame direction was less than the expected damage for an equivalent cast-in-place concrete structure. Rodriguez et al.¹⁴ investigated a half-scale, two-story precast concrete building incorporating a dual system and found that the precast concrete structural walls of the test structure controlled the force path mechanism and significantly reduced the lateral deformation demands in the precast concrete frames.

In general, multiple factors influence the seismic behavior of precast concrete structures. However, some factors lack significant investigation related to precast concrete structures' seismic behavior:

- Recent experimental investigations mainly focused on seismic behavior of the connections between precast

concrete beams and precast concrete columns. However, experimental investigations of the connections between cast-in-place concrete columns and composite concrete beams are scarce.

- It is reported that slabs have a significant influence on the negative flexural strength of the beam, which might alter the strength hierarchy of the connection and lead to column plastic hinging. However, there have been few studies on the behavior of precast concrete connections with slabs.

Due to the lack of experimental investigations and insufficient data about the seismic behavior of precast concrete connections, especially of precast concrete frames that could be used in seismic zones, the objectives of this investigation were to experimentally investigate the seismic behavior of a precast concrete, moment-resisting frame. Investigations of full-scale precast concrete connections—including an exterior connection, an interior connection, a T connection, and a knee connection—under cyclic loading were conducted. Also, a test of a half-scale, two-story, two-bay, precast concrete, moment-resisting frame under cyclic loading was conducted to evaluate the seismic behavior of precast concrete, moment-resisting frames. Behavior of the specimens was evaluated in terms of failure mode, stiffness degradation, energy dissipation, and displacement ductility.

Experimental program

The experimental program was conducted to assess the seismic behavior of moment-resisting, precast concrete frames composed of composite concrete beams and cast-in-place concrete columns. The selected precast concrete connections and the frame model were from a prototype frame building, which was a rectangular, six-story building

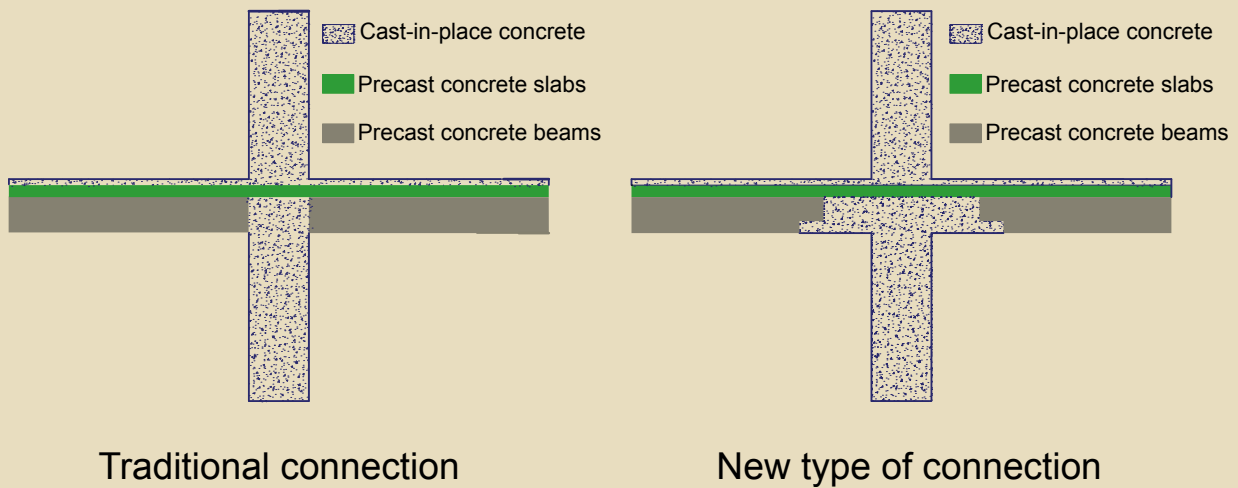


Figure 2. This schematic diagram compares the traditional connection with the new type of connection.

with plan dimensions of 9 m × 24 m (30 ft × 79 ft), 4 m (13 ft) column spacing, and 2.8 m (9 ft) story height. **Figure 1** presents the structural-plan layout of the prototype frame building.

The four connections and the frame model were designed according to a strong column–weak beam seismic design philosophy in accordance with the Chinese *Code for Seismic Design of Buildings*.¹⁵ All specimens had enough shear strength to prevent shear failure before flexural failure of the beam and column.

Description of test specimens

Compared with traditional precast concrete connections, one of the fundamental advantages of the precast concrete connections investigated in this paper (**Fig. 2**) was that the weak section in the beam was away from the most unfavorable position in which the moment and the shear were simultaneously maximum.

Specimens PCJ-1 and PCJ-2 represented an interior connection and an exterior connection in the first story, respectively. Specimens PCJ-3 and PCJ-4 were a T connection and a knee connection in the top story, respectively. All of the precast concrete connections consisted of a composite concrete beam and a cast-in-place concrete column.

In each specimen, five layers of horizontal joint hoops were equally spaced at 100 mm (4 in.) between the top and bottom longitudinal beam bars to prevent joint shear failure. To enhance the integrity of the precast concrete connections, several measurements were taken. A new type of composite beam was adopted (**Fig. 3**). The precast concrete beam overlaps the cast-in-place concrete section for a distance of 450 mm (18 in.) (which is also the depth of the beam h) from the column face along the beam. The column and beam end were cast at the same time (**Fig. 2**).

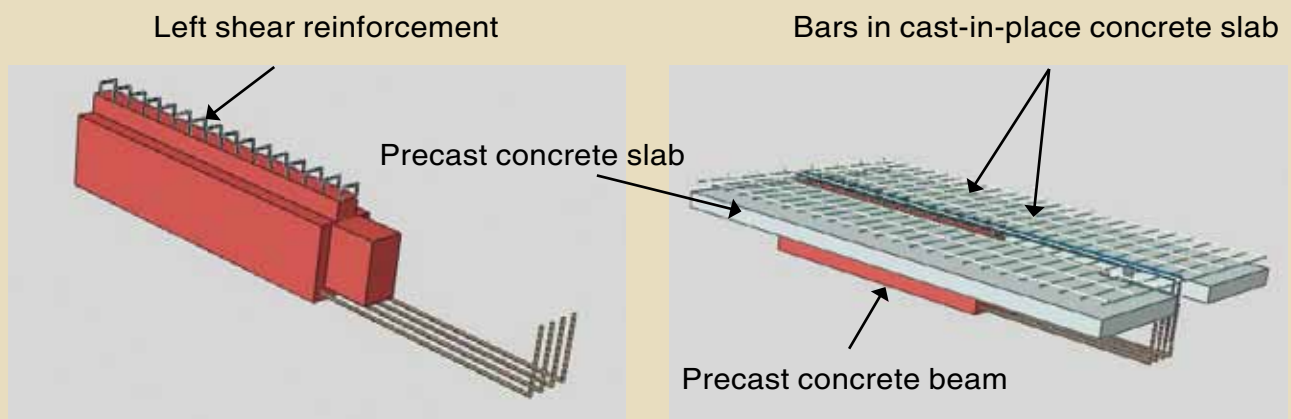


Figure 3. This schematic shows the composition of the precast concrete beam and composite beam. Note: For clarity, cast-in-place concrete is not shown.

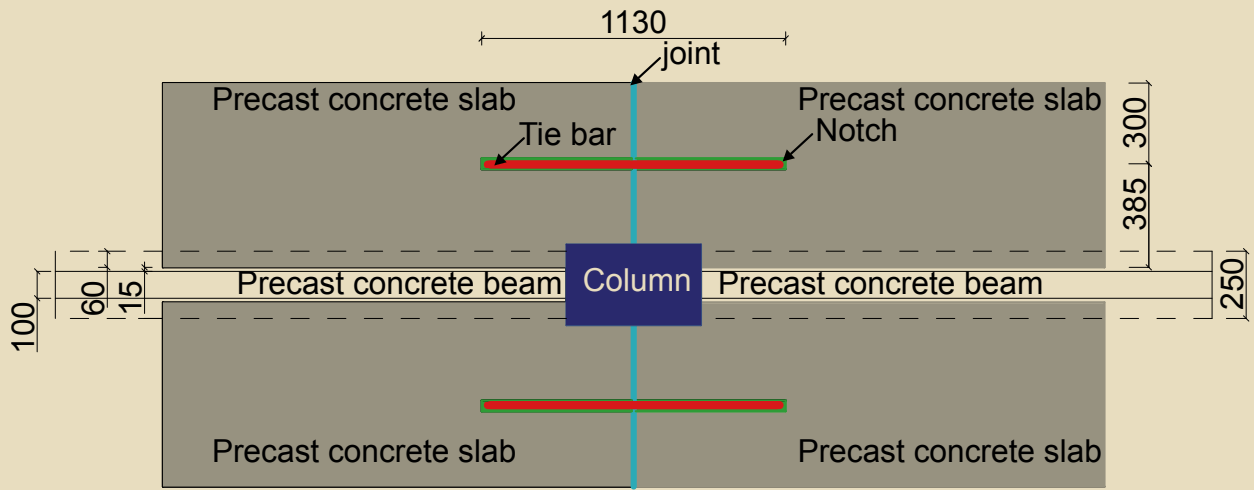


Figure 4. Notches were formed in the precast concrete slabs along the beam to place tie bars. Note: All dimensions are in millimeters. 1 mm = 0.0394 in.

The concrete shear key was formed at the beam end (Fig. 3), and the shear key and precast concrete slab were lightly brushed on the contact surface with an average roughness amplitude of 5 mm (0.20 in.). The notches were formed in the precast concrete slabs along the beam to place tie bars (Fig. 4), and the 560-mm-long (22 in.), 40-mm-wide (1.57 in.), 20-mm-deep (0.79 in.) notch provided enough development length for tie bars.

The composite beam consisted of a precast concrete invert-

ed-tee beam, precast concrete slab, and cast-in-place concrete slab that was reinforced with two D16 (D denotes bar diameter and the number is given in millimeters) deformed bars at the top and four D12 deformed bars at the bottom, which was identical in the four connections. The bottom steel bars, left anchored during precasting, protruded from the beam end and could extend into the joint core and were bent to form standard 90 deg hooks. The hooked longitudinal bars in the beam bottom passed through the full depth of the columns to achieve the code-required development

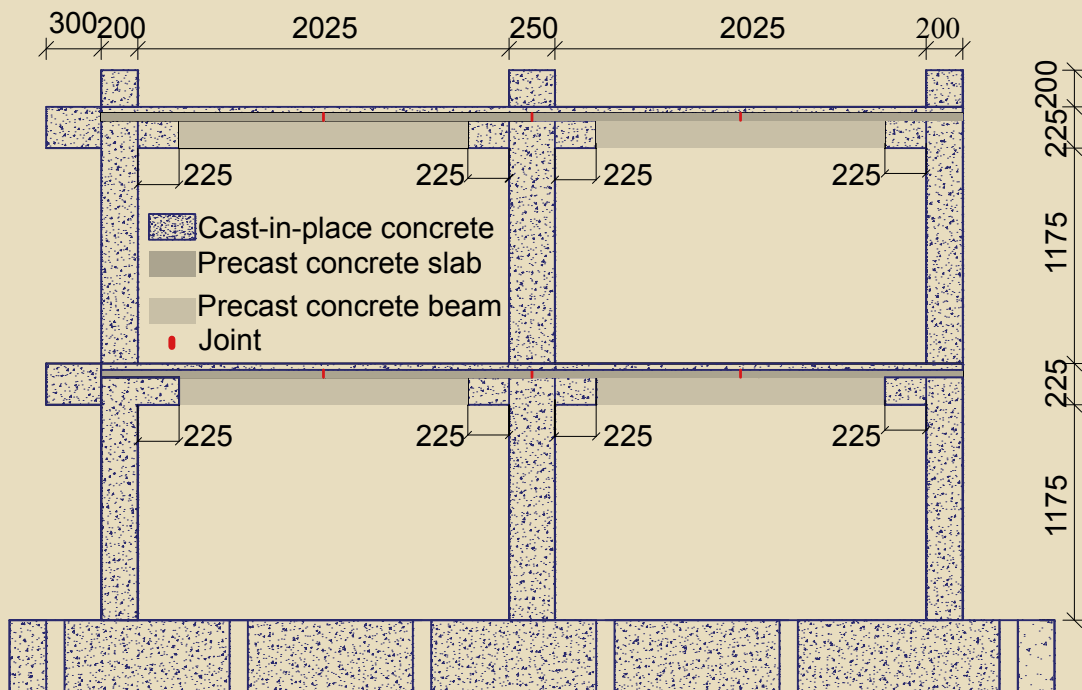


Figure 5. This schematic shows the locations of the precast concrete beams and slabs in the frame model. Note: All dimensions are in millimeters. 1 mm = 0.0394 in.

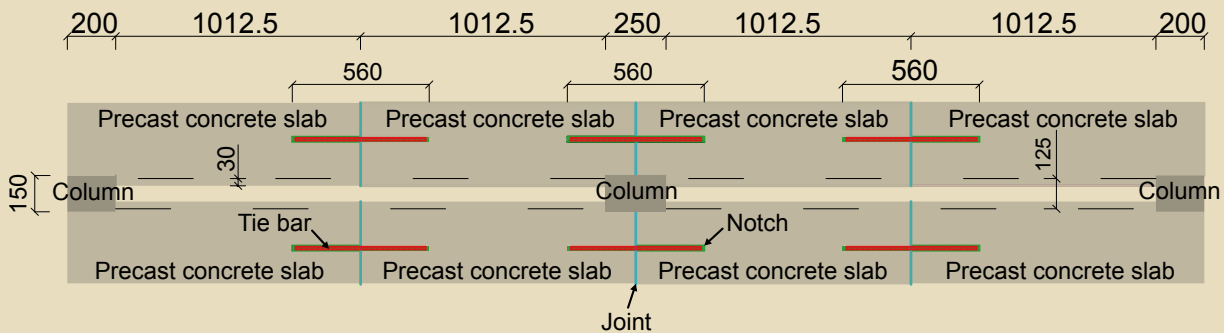


Figure 6. This diagram shows the location of tie bars and joints. Note: All dimensions are in millimeters. 1 mm = 0.0394 in.

length and avoid bond failure. In each specimen, the width and the thickness of the cast-in-place concrete slab were 1500 mm (59 in.) and 70 mm (2.8 in.), respectively.

The slab reinforcement consisted of eight D8 plain bars in the direction parallel to the precast concrete beam. The width of the precast concrete slab was 685 mm (27.0 in.), and slab reinforcements consisted of four D8 plain bars in the direction parallel to the precast concrete beam. The cast-in-place concrete slab was 70 mm (2.8 in.) thick and the precast concrete slab was 80 mm (3.2 in.) thick in the four connections. The lengths of the columns in all specimens were adjusted according to the height of the support.

For the interior connection, the column had a 300 mm × 500 mm (12 in. × 20 in.) cross section and the column longitudinal bars included six D16 and four D12 deformed bars, representing about 1.1% of the column gross area. The column of the exterior connection had a 300 mm × 400 mm (12 in. × 16 in.) cross section, and the column longitudinal reinforcement included six D16 and two D12 deformed bars, representing about 1.2% of the column gross area.

The column with the T connection had a 300 mm × 500 mm cross section, and the column longitudinal bars included eight D25 and four D12 deformed bars, representing about 2.9% of the column gross area. The column with the knee connection had a 300 mm × 400 mm cross section, and the column longitudinal reinforcement included eight D25 and two D12 deformed bars, representing about 3.5% of the column gross area. The flange width was one-third of the span length that is suggested in the *Code for Seismic Design of Buildings* from China and slightly larger than the effective flange width suggested by ACI 318-08.¹⁶

The frame model represented an inner-column strip along the south-north direction of the prototype structure (Fig. 1). The prototype frame (specimen PCF-1) was reduced to a half-scale model according to similitude law due to the experimental space constraints. In order to enhance

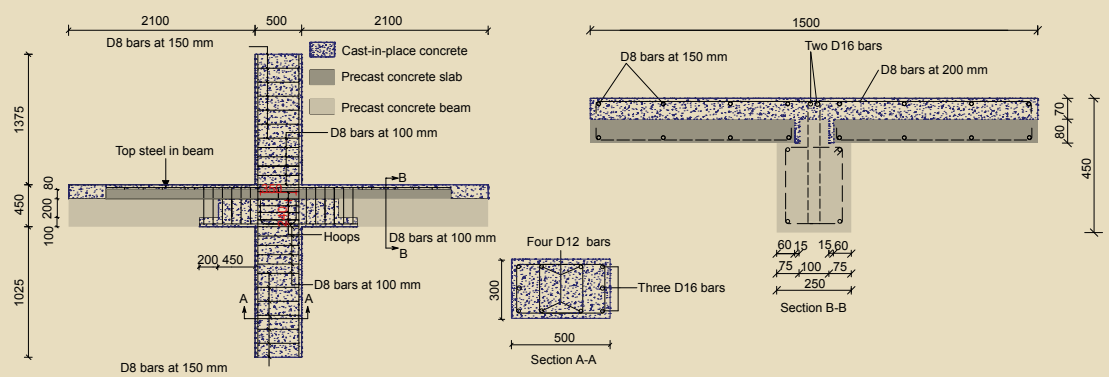
the integrity of the test frame, some measures similar to those taken in the precast concrete connections were taken. **Figure 5** depicts the layout of precast concrete beams and slabs. Specimen PCF-1 was cast upright to simulate actual detailing and constructing. **Figure 6** shows the notch and joint locations. The notch was 280 mm (11 in.) long, 20 mm (0.8 in.) wide, and 10 mm (0.4 in.) deep, which could provide enough development length for tie bars.

Figures 7 and **8** present dimensions and reinforcement details of the four connections and the frame model, respectively.

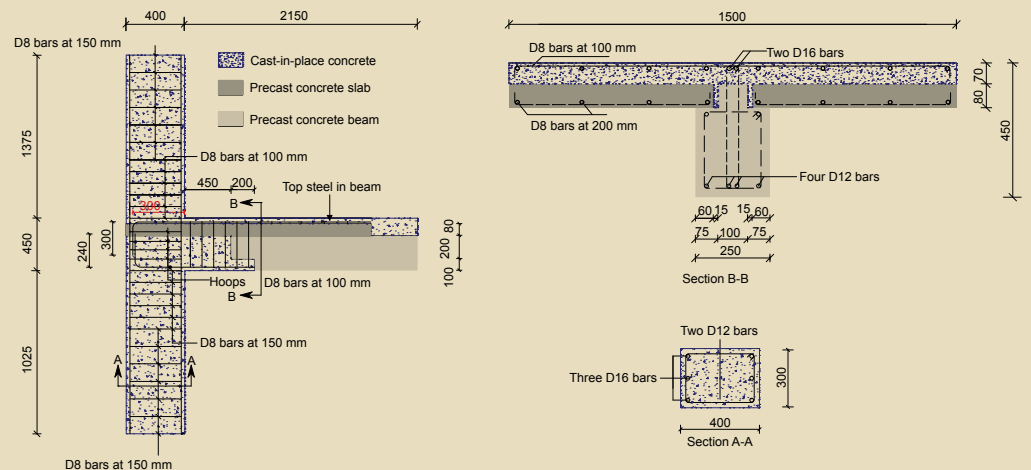
Construction process

The construction process of all four precast concrete connections was divided into two stages. First, the precast concrete components were prefabricated by a plant that specializes in manufacturing precast concrete. Second, the precast concrete components were assembled with cast-in-place concrete. Specific construction procedures were followed:

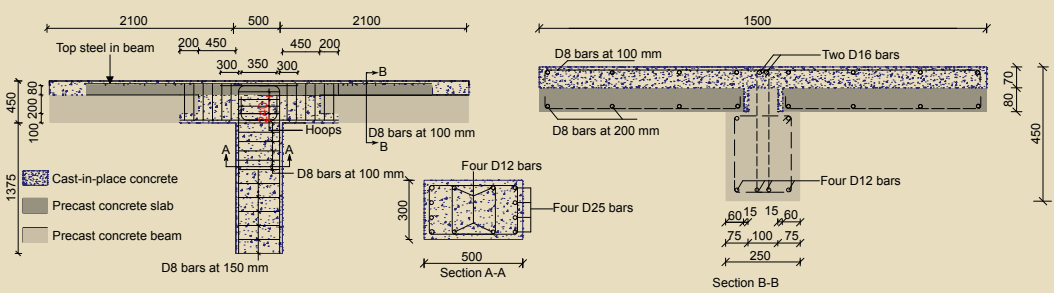
- The longitudinal bars and ties of columns were bound.
- Precast concrete beams were supported. The bottom steel bars, left anchored during precasting, extended into the joint core and were bent to form standard 90 deg hooks. The hooked bottom longitudinal bars passed through the full depth of columns to achieve the code-required development length and to avoid bond failure.
- Precast concrete slabs were placed on top of the inverted-tee precast concrete beams. The continuous top bars were then placed on top of the beams in the topping slab over the floor system and through beam-to-column joint core.
- Cast-in-place concrete with a maximum aggregate size of 25 mm (1 in.) was placed in the column and on



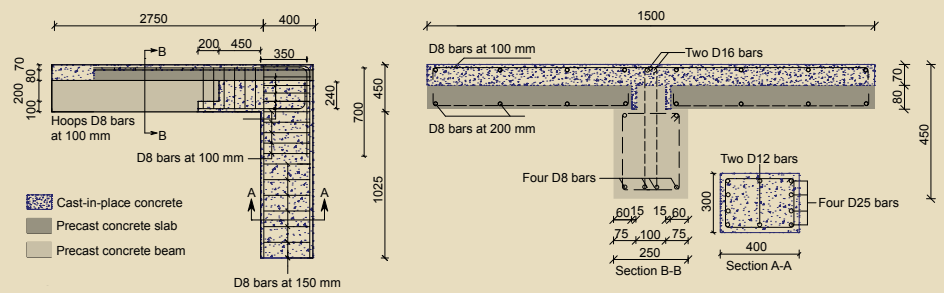
Specimen PCJ-1



Specimen PCJ-2



Specimen PCJ-3



Specimen PCJ-4

Figure 7. These diagrams show the geometry and steel details of the four connections. Note: All dimensions are in millimeters. 1 mm = 0.0394 in.

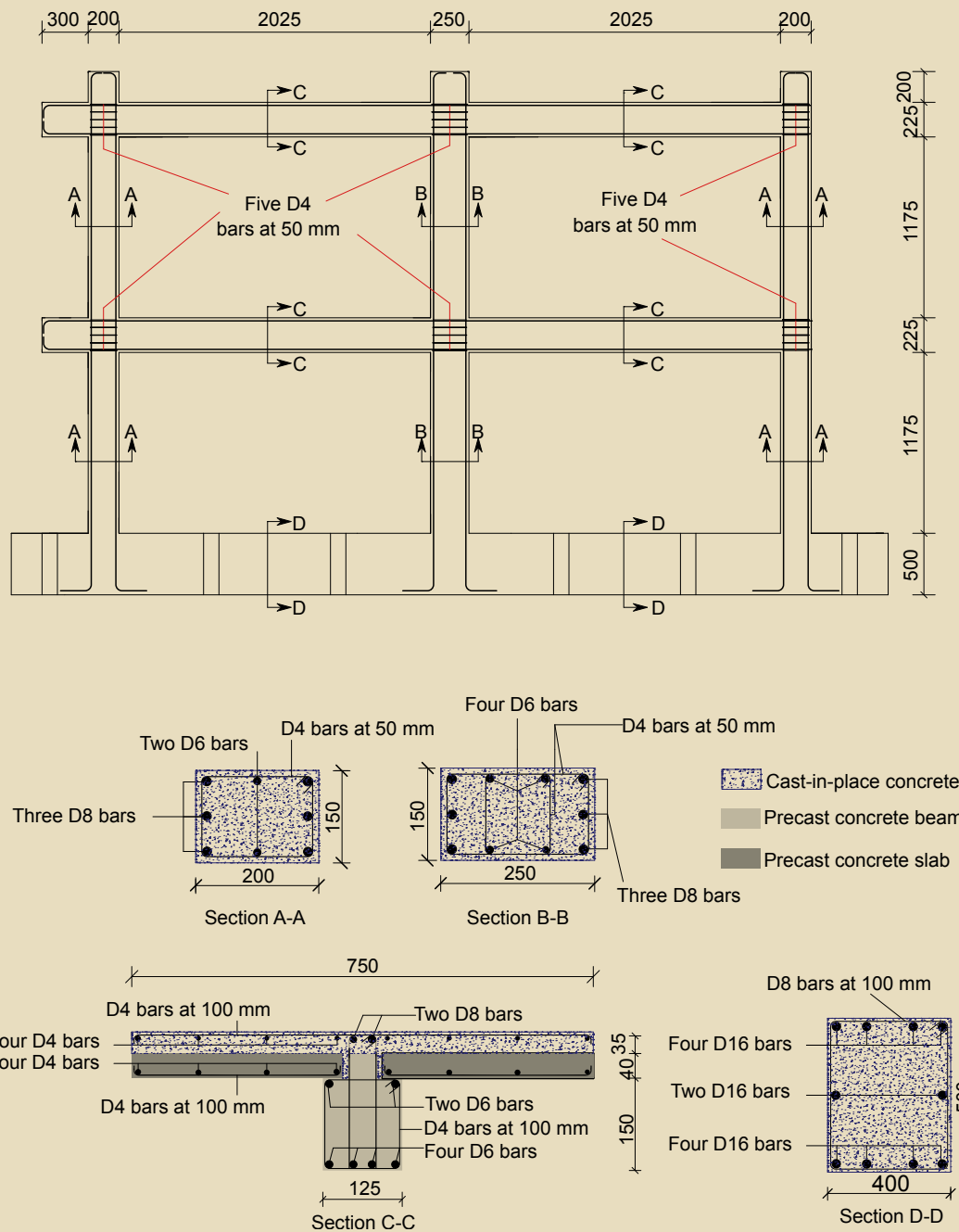


Figure 8. This schematic shows the geometry and steel details of the frame model specimen PCF-1. Note: All dimensions are in millimeters. 1 mm = 0.0394 in.

top of the precast concrete slabs, and internal vibration was used to consolidate the concrete.

The construction technology used in fabricating the precast concrete frames was similar to that used to fabricate the precast concrete connections, except that the ground beam was cast before binding the column bars.

In addition, the surface of the precast concrete members was clean and free of laitance. The specimens were moist-

cured for about 72 hr and then stored in the lab with wet-burlap wrapping until testing. Both of the specimens were cast upright.

The concrete was designed to achieve a cubic compressive strength of about 40 MPa (5.8 ksi) and a good workability to facilitate the handling of the mixture. **Tables 1** through **4** summarize the properties of the reinforcing steel and the concrete used in the connections and the frame model.

Table 1. Properties of reinforcing bars in connection specimens

	Bar diameter			
	D8	D12	D16	D25
Yield strength f_y , MPa	242	339	387	349
Ultimate strength f_u , MPa	395	510	588	554
Elastic modulus E_s , MPa $\times 10^5$	1.94	1.82	1.83	1.91
Elongation at fracture, %	32.5	31.6	27.5	22.1

Note: D = bar diameter in millimeters. 1 mm = 0.0394 in.; 1 MPa = 0.145 ksi.

Table 2. Material properties of concrete in connection specimens at the test

Specimens	PCJ-1		PCJ-2		PCJ-3		PCJ-4	
	CIP concrete	Precast concrete						
Cube strength f_{cu} , MPa	42.4	44.1	47.1	46.8	45.5	46.1	44.6	48.7
Spilt strength f_t , MPa	4.3	3.9	4.9	4.1	4.1	4.2	3.9	4.4
Concrete elastic modulus E_c , MPa $\times 10^4$	3.1	3.1	3.8	3.4	3.4	3.5	3.9	3.3

Note: CIP = cast-in-place. 1 MPa = 145 psi.

Table 3. Properties of reinforcing bars in the frame model

	Bar diameter				
	D8	D6	D4	D3.5	D2.77
Yield strength f_y , MPa	342	355	363	344	328
Ultimate strength f_u , MPa	415	586	414	448	400
Steel elastic modulus E_s , MPa $\times 10^5$	2.1	2.3	1.7	2.3	1.8
Elongation at fracture, %	14.8	12.9	22.5	15.3	13.5

Note: D = denotes bar diameter in millimeters. 1 mm = 0.0394 in.; 1 MPa = 0.145 ksi.

Table 4. Material properties of concrete in the frame model

PCF-1	Cast-in-place concrete	Precast concrete
Cube strength f_{cu} , MPa	48.7	49.8
Spilt strength f_t , MPa	3.9	3.7
Concrete elastic modulus E_c , MPa $\times 10^4$	3.4	3.5

Note: 1 MPa = 0.145 ksi.

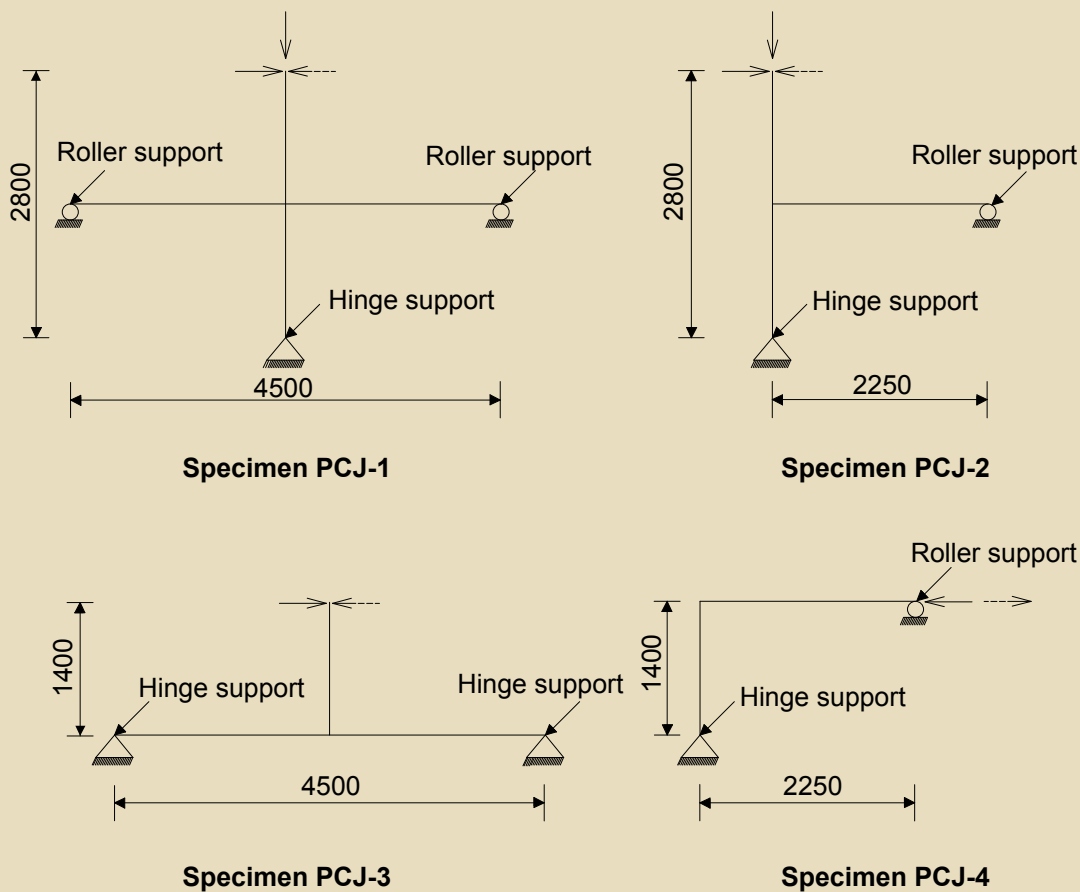


Figure 9. This diagram shows the boundary conditions for connection specimens. Note: All dimensions are in millimeters. 1 mm = 0.0394 in.

Test setup and loading sequence and measurement

All test specimens were constructed and tested at the Tongji University Structural Engineering Laboratory. For the four connections, the adopted geometry of the investigated specimens represented the beam-to-beam inflection points and column-to-column inflection points (points of zero moment) that existed at the midspans of beams and columns when a frame was subjected to earthquake-induced lateral loads. **Figure 9** shows the boundary conditions for the four connections.

Except for specimen PCJ-3, which was tested in an inverted position with respect to the existing position in the frame, the connections were supported in a vertical position. The bottoms of the columns in specimens PCJ-1, PCJ-2, and PCJ-4 were supported by universal pins, and the beam end was designed as a horizontal roller support, which was designed to realize the beam end’s horizontal translation and rotation and restrict its vertical displacement. The two beam ends of specimen PCJ-3 were supported by hinge supports, and the point of load at the

column end was free to rotate in the loading plane. These boundary conditions were chosen to model actual conditions.

For specimens PCJ-1 and PCJ-2, the constant axial load was applied to the tops of the columns through a vertical 10,000 kN (2250 kip) hydraulic actuator that could automatically trace the column top when loading to consider the P-delta effect. The axial compressive ratio was 0.4 for specimen PCJ-1 and 0.3 for specimen PCJ-2, representing vertical load experienced in the first story of the prototype building.

After the application of the column axial load, the lateral cyclic loading was applied at the top of the column through a horizontal 3000 kN (675 kip) hydraulic actuator according to loading history. The loading process of specimens PCJ-3 and PCJ-4 was similar to that of the other two connections, neglecting the column axial load. Because specimens PCJ-2 and PCJ-4 were not symmetrical in the loading plane, a steel bracket was installed near the top of the column to guide specimen displacements along the loading direction only.

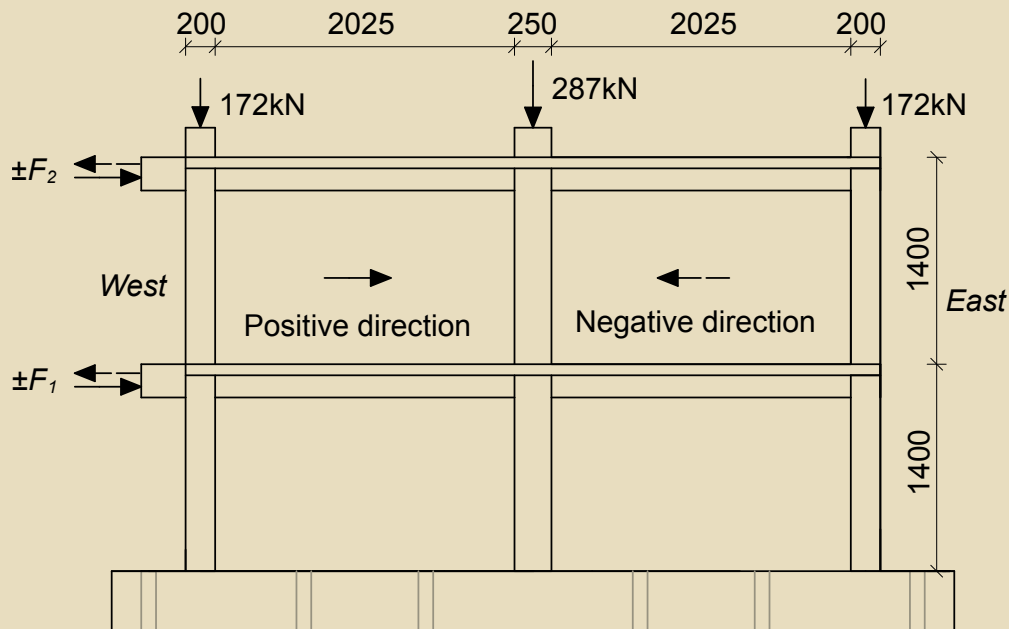


Figure 10. Lateral loads F_1 and F_2 were applied at the first and second levels of the structure, respectively. Note: Dimensions not listed are in millimeters. 1 mm = 0.0394 in.; 1 kN = 0.225 kip.

The frame model, specimen PCF-1, was tested under constant vertical loads (an axial compressive ratio of 0.3 for the two exterior columns and 0.4 for the middle column), which represented the axial load due to live and dead loads of the upper story in the prototype structure. The vertical loads were applied to three column tops by using three identical hydraulic actuators attached to the steel girder through a sliding cart, which could automatically trace the column top when loading to consider the P-delta effect.

A horizontal 3000 kN (675 kip) hydraulic actuator mounted to a rigid reaction frame was applied to the lateral load. The lateral force distribution was maintained in the shape of an inverted triangle by using the whiffletree. Lateral loads F_1 and F_2 were applied at the first and second levels of the structure, respectively (**Fig. 10**). The ratio of F_2 to F_1 was held constant throughout the test, with a value of 2.0, which reflected the distribution of horizontal seismic force along the structure's height. Figure 10 shows the test setup and the positive and negative directions of loading.

Figure 11 shows the loading history used in this study. The loading history was divided into two phases: a load-controlled cycle and a displacement-control phase, which consisted of displacement cycles of increasing magnitude at 0.5%-story-drift increments, with three cycles applied at each new drift level.

Applied loads and lateral displacements were monitored through load cells and linear variable-differential transducers (LVDTs), respectively. Electrical resistive strain gauges were

mounted on selected locations of the longitudinal and transverse reinforcement of columns and beams. A data-acquisition system continually recorded the readings. In addition, the crack propagation in each specimen was highlighted, and the progress of damage was photographed at each peak.

Experimental results and discussion

Behavior and failure pattern of connections

The cracking pattern monitored throughout the tests served as an indicator of the nature and the progress of the failure and provided useful information regarding the failure mechanism for each specimen. **Figures 12** and **13** show the final crack patterns observed at the end of testing of the four connections and the frame, respectively.

Specimen PCJ-1 The first fine flexural crack occurred in the beam at a distance of 700 mm (27.6 in.) from the face of the column at a load of 46.3 kN (10.4 kip). The initial cracking location was the interface between cast-in-place concrete and precast concrete. At a drift of 0.53%, the specimen reached the yield state that was defined according to the criteria used by Park¹⁷ for equivalent elastoplastic energy absorption and its maximum load-carrying capacity at a drift of 1.0%.

The load-carrying capacity did not severely degrade until a drift of 2.94% with light pinching. Vertical and horizontal

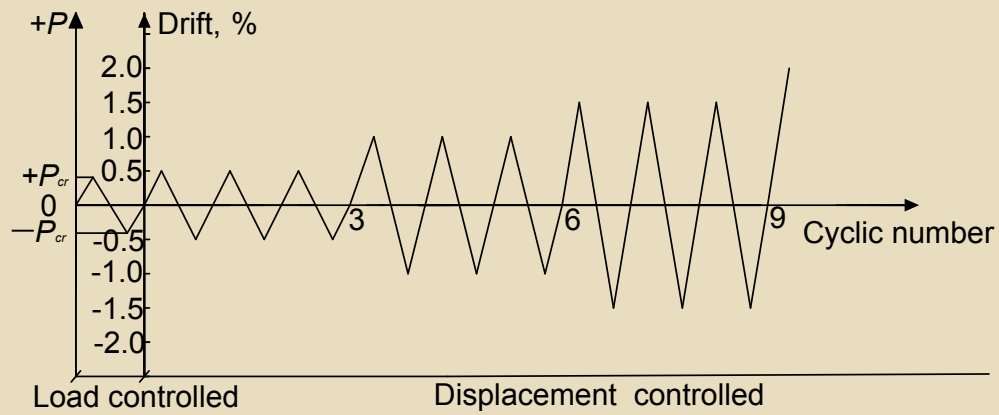


Figure 11. This graph shows the cyclic-loading history used in this study. Note: P = load; P_{cr} = cracking load.



Specimen PCJ-1



Specimen PCJ-2



Specimen PCJ-3



Specimen PCJ-4

Figure 12. These photos show the crack patterns and failure modes of four connections at the end of the test.

cracks appeared at the bottom of the beam end at a drift of 1.0% as a result of the bars slipping. Diagonal shear cracks appeared in the joint at a drift of 2.0%. Flexural cracks on precast concrete beams were uniformly distributed along the entire length of the beam.

Specimen PCJ-2 The first flexural crack occurred in the beam at a distance of 700 mm (27.6 in.) from the face of the column at a load of 20.9 kN (4.7 kip). During the seventh load cycle, diagonal shear cracks developed in the joint region. With progressive loading, diagonal shear cracks propagated in the joint zone. Repetition of cycles led to opening and closing of the formed cracks, which caused a softening of concrete and a decrease in strength.

Specimen PCJ-3 At a lateral load of 61.1 kN (13.7 kip), a hairline crack occurred at the beam-column interface, which was about 700 mm (27.6 in.) from the face of the column. Initial joint shear cracks were observed during a 1.0% drift cycle. The joint cracks were diagonally inclined, and they intersected one another due to the cyclic loading.

As the story drift increased, the joint shear capacity did not obviously deteriorate and no joint concrete spalled in the joint face throughout the test. Specimen PCJ-3 showed many beam flexural cracks and reached its maximum load-carrying capacity at a drift of 2.0%. During the 5.0% drift cycle, the test was halted due to reinforcement fracture at the bottom of the beam end, exhibiting a strong column–weak beam failure mechanism.

Specimen PCJ-4 The first flexural crack occurred in the column at a load of 70.3 kN (15.8 kip), and it showed beam flexural cracks and then diagonal shear cracks in the joint at a drift of 1.0%. As the story-drift level increased, cracks in the joint panel progressed and the joint shear capacity gradually deteriorated. Specimen PCJ-4 showed many flexural-shear cracks in the beam and column and reached its maximum load-carrying capacity at a drift of 2.0%. The test was halted at a drift of 5.0% because the reinforcement fractured at the bottom of the beam end.

Generally, the four connections, as expected, developed plastic hinges in the vicinity of the beam-joint interfaces without severe damage in the joint and exhibited strong column–weak beam failure mechanisms. This desired failure mechanism led to ductile failure in the structure. Concrete cracking damage was concentrated in the vicinity of the joint region, especially in the beams' plastic-hinge zones. At the final stage of loading, severe spalling of large pieces of cover concrete was observed in the fixed beam end during cyclic loading in each connection. There were no horizontal cracks observed in the failure cross section. The number of the column cracks in specimens PCJ-3 and PCJ-4 was more than that of specimens PCJ-1 and PCJ-2. Based on the measured longitudinal bar strains in the beam, the plastic hinge length in the beam end was less than $1.5h$.



Figure 13. This photo shows the final failure patterns of the frame model specimen PCF-1 at the end of the test.

In addition, the slip between the precast concrete beam and the precast concrete slab and the slip between the precast concrete slab and the cast-in-place concrete slab were measured during the test of the four connections. When the connection reached the yield state, the slip between the precast concrete slab and the cast-in-place concrete slab in the four connections was less than 0.1 mm (0.004 in.), and the slip between the precast concrete beam and the precast concrete slab was less than 0.09 mm (0.0035 in.), except for the slip between the precast concrete beam and the precast concrete slab in specimen PCJ-4, which was 0.4 mm (0.016 in.). When reaching peak load, the slip between the precast concrete slab and the cast-in-place concrete slab was less than 0.4 mm in specimen PCJ-4 and less than 0.11 mm (0.0043 in.) in the other three connections. The slip between the precast concrete beam and precast concrete slab in specimens PCJ-2 and PCJ-4 was less than 0.06 mm (0.0024 in.). However, the slip between the precast concrete beam and the precast concrete slab in specimens PCJ-1 and PCJ-3 was about 0.65 mm (0.025 in.). These results showed that the slip in the composite beams in this type of precast concrete frame was little, and the measures (that is, roughing the contact surface and including the notch to place tie bar) taken to improve the integrity of the cross section in the composite beam were effective.

Behavior and failure pattern of specimen PCF-1

When the total lateral load reached 77.0 kN (17.3 kip) in the positive direction, the first hairline flexural crack occurred at the west beam end adjacent to the middle column in the first story. When the total lateral load reached 70.0 kN (15.8 kip) in the negative direction, a new fine flexural crack occurred at the east beam end in the first story. Both of the fine flexural cracks were basically symmetrical about the middle column.



Column base



Top of beam end

Figure 14. The photos indicate the typical failure patterns at the beam ends and column ends in the frame model specimen PCF-1.

The first plastic hinge occurred at the beam end in the first story at a total lateral load of 115.3 kN (25.9 kip), the corresponding roof drift was 0.52%, and many new cracks appeared and progressed when loading. Specimen PCF-1 reached its yield state when the total lateral load reached 195 kN (43.9 kip) at a roof drift of 0.6% in the positive direction, and the total lateral load reached 185 kN (41.6 kip) at a roof drift of 0.8% in the negative direction.

The yield state was defined according to the method used by Park. At a roof drift of 2.0%, its maximum load of 217.3 kN (48.9 kip) was attained and the west column base was damaged. The load-carrying capacity decreased gradually after reaching the peak load with increasing roof drift and dropped 15% at a roof drift of 3.1% in the positive direction and at a roof drift of 3.2% in the negative direction. The test was terminated at a roof drift of 3.5% and a load of 161 kN (36.2 kip) because the load-carrying capacity deteriorated severely and the column bases were severely damaged. In addition, cover concrete was lost, and longitudinal reinforcements and ties were exposed at the column bases in the first story.

There were a few hairline cracks in the first-story joints, and the strains of all of the joint hoops stayed in the elastic stage, indicating that the shear strength of the joints was sufficient to maintain elastic behavior. **Figure 14** shows the ultimate damage states of the columns and beams. **Figure 15** depicts the measured sequences of hinge formation. The following results were observed:

- Under cyclic loading, the first plastic hinge occurred at the first-story beam end, and when plastic hinges at the beam ends developed to some extent, the plastic hinge began to occur at the column ends.

- The frame, as expected, exhibited a mixed side-sway mechanism and failed due to concrete crushing and buckling of longitudinal bars as a result of plastic hinges at the fixed column bases, and it achieved the design objectives.

P-delta hysteretic response

Figures 16 and **17** show the lateral load-versus-story drift hysteresis curves of all four connections and the frame model, respectively. At the earlier stage, the four connections exhibited a stable load-versus-story drift hysteretic response, and then slight pinching (the middle part of each hysteretic loop was relatively narrow) could be noticed in the hysteresis loops of the four connections, primarily due to joint diagonal cracking and beam-end cracking. The hysteresis curves of specimens PCJ-3 and PCJ-4 exhibited more pronounced pinching than the other two connections. The areas of hysteresis loops gradually became larger as story drift increased and plastic hinge formed in the beam end, indicating good energy-dissipation capacity.

For specimens PCJ-2 and PCJ-4, the hysteresis curves were not symmetrical due to the presence of the concrete slab, and there were obvious differences in load-carrying capacity in both directions for which the concrete slab was engaged in tension. For specimens PCJ-1 and PCJ-2, the overall response was mainly dominated by beam-end rotations due to the minor nature of the damage in the joint core. However, the characteristics of the hysteretic response of specimens PCJ-3 and PCJ-4 were dominated by beam-end rotations and the degree of damage in the joint regions because the degree of damage in the joint regions of these two connections was more severe than that of the other connections.

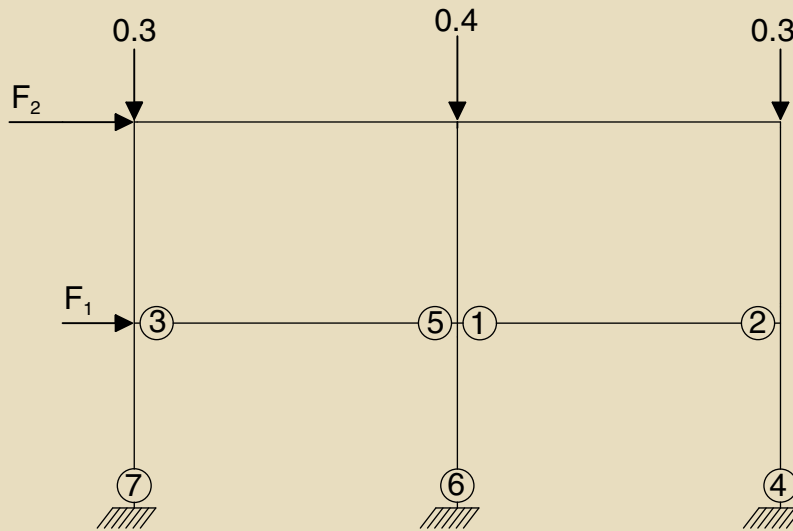
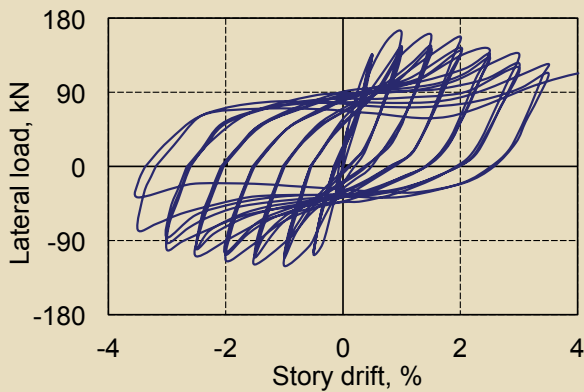
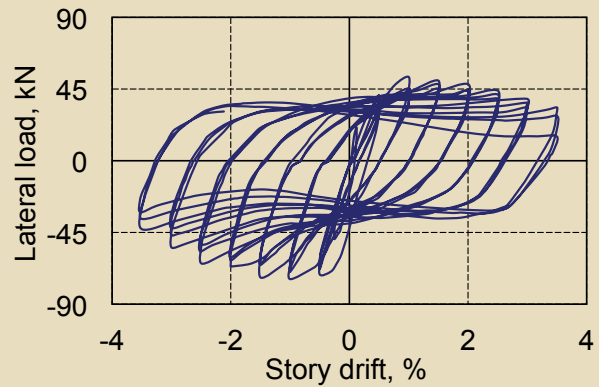


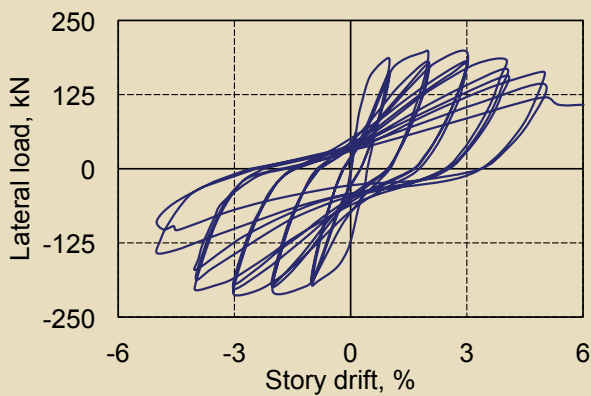
Figure 15. This diagram depicts the measured sequence of hinge formation in the frame model specimen PCF-1. Note: F_1 = lateral load applied to first level of test structure; F_2 = lateral load applied to second level of test structure.



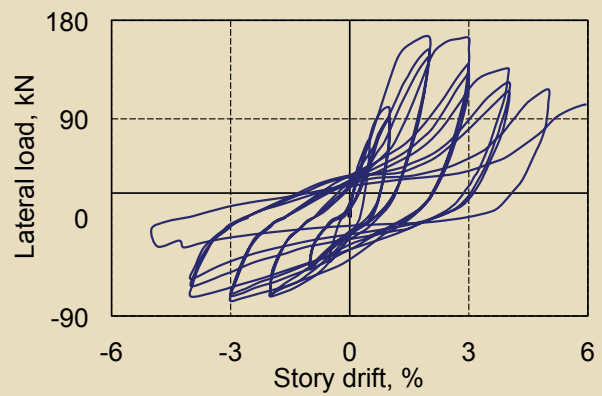
Specimen PCJ-1



Specimen PCJ-2

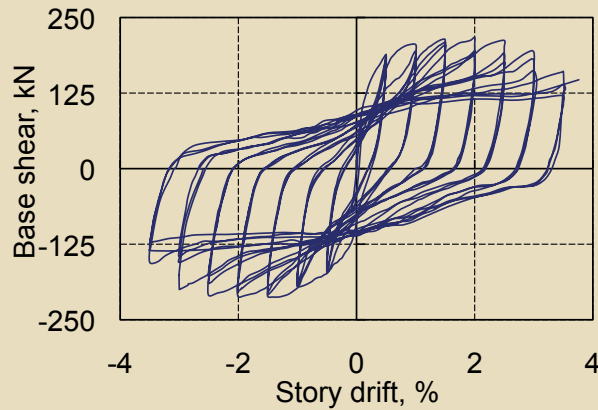


Specimen PCJ-3

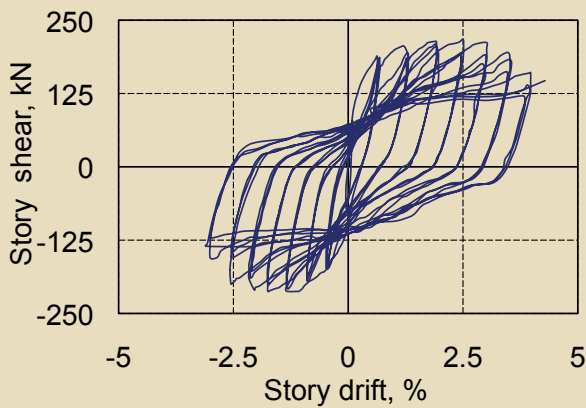


Specimen PCJ-4

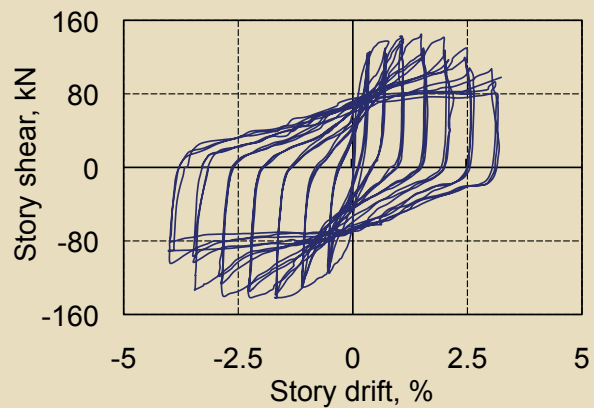
Figure 16. These graphs show the hysteresis curves of connection specimens. Note: 1 kN = 0.225 kip.



Roof



First story



Second story

Figure 17. The graphs show the hysteresis curves for the frame model specimen PCF-1. Note: 1 kN = 0.225 kip.

Specimen PCF-1 exhibited a stable load-versus-drift hysteretic response, and the areas of hysteresis loops gradually became larger with increasing roof drift and plastic hinge

formation in beam ends and column ends, showing good energy-dissipation capacity. The stiffness of the frame degraded after the cracking point and the stiffness degradation was severe after reaching yield point, but the overall behavior of the frame was stable without abrupt strength degradation. Slight pinching was noticed in the hysteretic loops after the roof-drift level of 1.0%, primarily due to column-end and beam-end cracking and concrete softening and bond slip.¹⁸ The maximum load of the first cycle was higher than that of the other two cycles at the same roof-drift level, showing strength degradation. The load-carrying capacity gradually decreased after a roof drift of 2.0%, and specimen PCF-1 exhibited good displacement ductility.

Displacement ductility and deformability

The displacement ductility is the ratio of the maximum deformation that a structure or element can undergo without a significant loss of initial yielding resistance to the initial yield deformation. However, it was not easy to determine

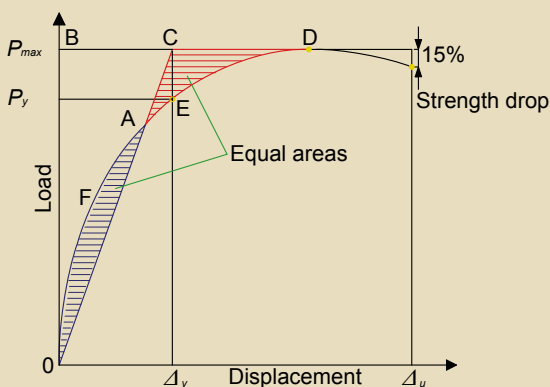


Figure 18. The load-versus-displacement envelope curve was used to define the yield and maximum displacements according to the criteria for equivalent elasto-plastic energy absorption. Note: P_{max} = peak load; P_y = yield load; Δ_u = ultimate displacement; Δ_y = yield displacement.

Table 5. Displacement ductility values of connection specimens

Specimen	Direction	Δ_{cr} mm	Δ_y mm	Δ_{max} mm	Δ_u mm	Δ_u/Δ_y	Δ_y/Δ_{cr}
PCJ-1	Positive	0.08	14.82	28.00	82.3	5.55	185.25
	Negative	0.13	14.16	28.00	82.7	5.84	108.92
PCJ-2	Positive	2.87	16.48	28.00	67.93	4.12	5.74
	Negative	7.11	17.13	28.00	72.64	4.24	2.41
PCJ-3	Positive	1.86	11.38	28.00	66.48	5.84	6.12
	Negative	1.21	13.09	42.00	62.19	4.75	10.82
PCJ-4	Positive	6.64	22.47	28.00	53.79	2.39	3.38
	Negative	7.20	24.61	42.00	62.63	2.54	3.42

Note: Δ_{cr} = displacement corresponding to cracking load; Δ_{max} = displacement corresponding to peak load; Δ_u = ultimate displacement; Δ_y = yield displacement. 1 mm = 0.0394 in.

Table 6. Displacement ductility values of the frame model

Parameter	Direction	Δ_{cr} , mm	Δ_y mm	Δ_{max} , mm	Δ_u , mm	Δ_u/Δ_y	Δ_y/Δ_{cr}	Δ_{max}/Δ_y
Global	Positive	2.24	17.26	56	87.49	5.04	7.71	3.24
	Negative	2.31	21.56	56	90.33	4.19	9.33	2.60
First story	Positive	1.35	10.67	35.04	51.09	5.71	7.90	3.28
	Negative	1.29	8.62	24.50	38.48	4.46	6.68	2.84
Second story	Positive	1.52	6.73	20.96	36.7	5.45	4.43	3.11
	Negative	1.66	10.86	31.50	51.83	4.77	6.54	2.90

Note: Δ_{cr} = displacement corresponding to cracking load; Δ_{max} = displacement corresponding to peak load; Δ_u = ultimate displacement; Δ_y = yield displacement. 1 mm = 0.0394 in.

yield points for the specimens directly from the lateral load-versus-displacement curves. For each specimen, the load-versus-displacement envelope curve was used to define the yield and maximum displacements according to the criteria for equivalent elastoplastic energy absorption used by Park (Fig. 18). The ultimate displacement Δ_u corresponded to a 15% drop of the peak load. The displacement ductility was calculated from the ratio of ultimate displacement to yield displacement Δ_u/Δ_y . Tables 5 and 6 summarize the displacement ductility of the four connections and the frame model, respectively, showing both the displacement corresponding to the cracking load Δ_{cr} and the displacement corresponding to the peak load Δ_{max} .

The average displacement ductility of specimens PCJ-1, PCJ-2, PCJ-3, and PCJ-4 was 5.7, 4.2, 5.3, and 2.5, respectively. These results indicated that the four connec-

tions behaved in a ductile manner. The interior connection exhibited larger displacement ductility than in the other three connections. The displacement ductility of the knee connection was the poorest among these specimens, and it was necessary to take some measures to improve the ductility of the knee connection. The ratio of Δ_y/Δ_{cr} for the interior connection was larger than that of the exterior connection, which indicated that the safety margin of the interior connection was larger than that of the exterior connection after cracking.

The global displacement ductility factor of specimen PCF-1 was about 4.6, and the interstory displacement ductility factors were both about 5.1, showing that the frame model exhibited good ductility. The ratio of Δ_y/Δ_{cr} was more than 4.4, indicating that the frame model had a good safety margin.

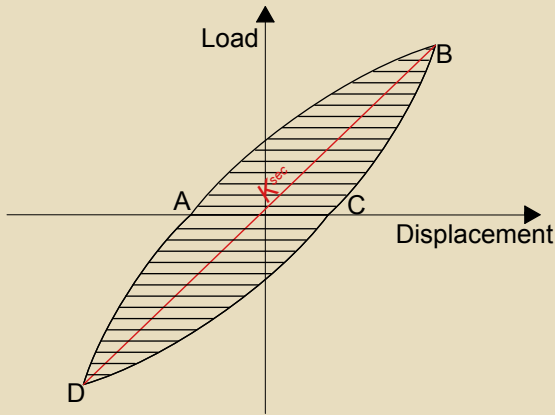


Figure 19. The secant stiffness was calculated using a straight line between the maximum load and corresponding displacement points for the positive and negative directions in a load cycle. Note: K_{sec} = secant stiffness.

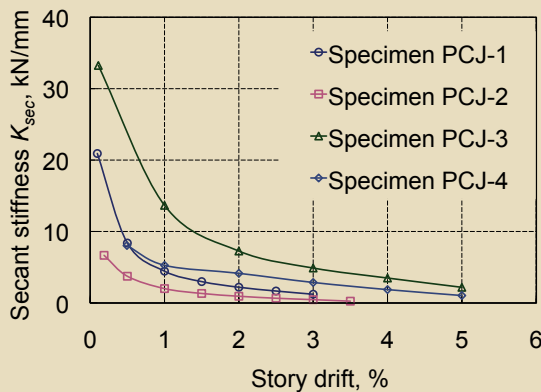


Figure 20. This graph compares the stiffness degradation with story drift for the four connection specimens. Note: 1 kN/mm = 5.71 kip/in.

Stiffness degradation

The rate of stiffness degradation is a precise parameter that can be used to gauge the specimen's overall response. In order to assess stiffness degradation, the secant stiffness was computed for each loading cycle at a particular drift level. The secant stiffness was calculated using a straight line between the maximum load and corresponding displacement points for the positive and negative directions in a load cycle (Fig. 19). Figures 20 and 21 plot the degradation in stiffness versus story drift. Stiffness continuously decreased with increasing story drift due to the increase in cumulative damage in columns and beams throughout the test, and each specimen experienced severe stiffness degradation at the end of the test.

Stiffness degradation was faster before the drift of 1% for all specimens, which was due to concrete cracking and reinforcement yielding in this stage. At a drift of 2.0%, a reduction of 89.5%, 86.1%, 78.2%, and 48.4% of the initial

stiffness was recorded for specimens PCJ-1, PCJ-2, PCJ-3, and PCJ-4, respectively. This showed that the stiffness degradation of the interior joint was more severe than that of the exterior connection and that the T connection was more severe than that of the knee connection. When the frame model reached its maximum load-carrying capacity at a drift of 2.0%, the stiffness dropped about 87%, 76%, and 85% for the first story, second story, and global frame, respectively, showing that stiffness degradation was severe. The initial stiffness of the second story and the global frame were close and lower than that of the first story.

Energy-dissipation capacity

The good energy-dissipation capacity indicated the capacity of the structure to perform satisfactorily in the inelastic range. It also indicated that the energy-dissipation capacity of the structure should be larger than the energy demand. A desirable behavior for a beam-column connection under cyclic loading implies a sufficient amount of energy dissipation without a substantial loss of strength and stiffness. The amount of energy dissipated during a load cycle at a particular drift level was calculated as the area enclosed by the load-displacement hysteretic loop (Fig. 19). The cumulative energy dissipated at a particular story-drift level was determined by summing the energy dissipated per loop to that point, and Figures 22 and 23 plot it versus the drift.

All four connections and the frame model exhibited similar patterns of energy dissipation. The energy-dissipation capacity of the test specimens increased as the drift increased. During the first cycle, the amount of energy that dissipated was small, showing that the test specimen stayed in the elastic stage. When the test specimens entered the elastoplastic stage, the amount of the dissipated energy of the test specimens increased with the increasing damage. After reaching the peak load, the load-carrying capacity of the test specimens began to gradually decrease, but the energy-dissipation capacity still slowly increased.

The energy-dissipation capacity of the interior connection was greater than that of the exterior connection. This could be because only one beam was in the exterior connection. The energy-dissipation of the test specimens is thought to be mainly dependent on the beam end hinging because the column and joint did not have any obvious damage. The energy dissipation capacity of the two top-story connections was lower than that of the two bottom-story connections, and the energy-dissipation capacity of the knee connection was the lowest.

Conclusion

This study was performed as one phase of an extensive research program on the seismic behavior of precast concrete frames. Based on the experimental results described in this paper, several conclusions were drawn:

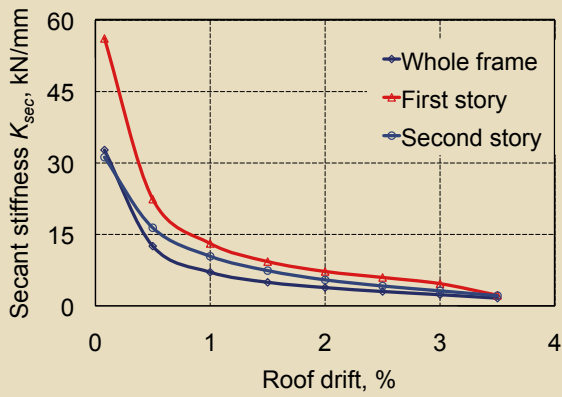


Figure 21. This graph compares the stiffness degradation with roof drift for the frame model specimen PCF-1. Note: 1 kN/mm = 5.71 kip/in.

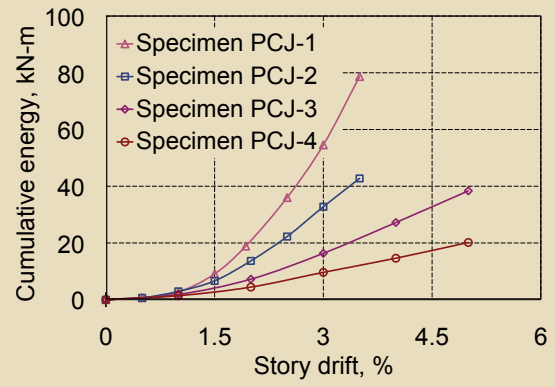


Figure 22. This graph shows the cumulative energy dissipation for the connection specimens. Note: 1 kN-m = 740 lb-ft.

- Putting the weak section in the beam to avoid the most unfavorable position is an effective measure. For the four connections, the initial cracking location was the interface between cast-in-place concrete and precast concrete in the beam end, but the severe damage occurred in the beam end.
- Roughing the surface of the precast concrete slab and left shear stirrups is an effective measure to ensure composite action. The slip in the composite beam was small, and the composite action between the precast concrete slab and cast-in-place concrete slab was good.
- Knee connections are less effective connections compared with interior, exterior, and T connections. As expected, all four connections underwent beam hinging around the beam-column interfaces before they reached their maximum load-carrying capacity. They also exhibited a strong column–weak beam failure mechanism. They failed due to concrete crushing and rupture of longitudinal bars as a result of plastic hinges at the beam fixed end. However, the knee connection also formed the hinge in the beam end. The joint damage was heavier than that of the other connections. The seismic behavior of knee connections with slabs requires additional investigations.
- Precast concrete connections and frames can perform satisfactorily in seismic conditions with respect to strength, ductility, and energy-dissipation capacity. The results of this investigation could provide some valuable information to expand the market for the frames that consist of composite concrete beams and cast-in-place concrete columns in high seismic zones.

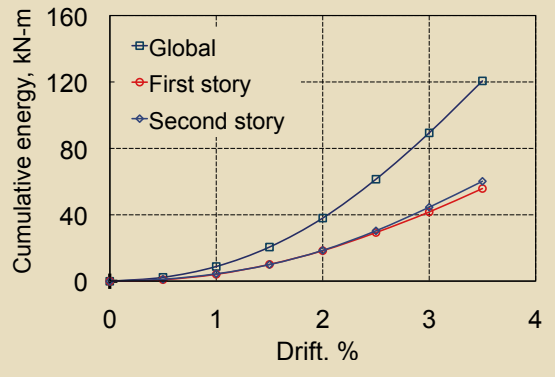


Figure 23. This graph shows the cumulative energy dissipation of the frame model specimen PCF-1. Note: 1 kN-m = 740 lb-ft.

Acknowledgments

The authors gratefully acknowledge the financial support provided by the National Natural Science Foundation of China under grant no. 50878167, Shanghai Urban-Rural Development and Transport Commission under Grant No. 2009-001-004, and Vanke Co. Ltd.

References

1. Ochs, J. E., and M. R. Ehsani. 1993. Moment Resistant Connections in Precast Concrete Frames for Seismic Regions. *PCI Journal*, V. 38, No. 5 (September–October): pp. 64–75.
2. Park, R. 2002. Seismic Design and Construction of Precast Concrete Buildings in New Zealand. *PCI Journal*, V. 47, No. 5 (September–October): pp. 60–75.

3. Korkmaz, H. H., and T. Tankut. 2005. Performance of a Precast Concrete Beam-to-Beam Connection Subject to Reversed Cyclic Loading. *Engineering Structures*, V. 27, No. 9 (August): pp. 1392–1407.
4. Park, R., and D. K. Bull. 1986. Seismic Resistance of Frames Incorporating Precast Prestressed Concrete Beam Shells. *PCI Journal*, V. 31, No. 4 (July–August): pp. 54–93.
5. French, C. W., O. Amu, and C. Tarzikhan. 1989. Connections between Precast Elements—Failure outside Connection Region. *Journal of Structural Engineering*, V. 115, No. 2 (February): pp. 316–340.
6. French, C. W., M. Hafner, and V. Jayashankar. 1989. Connections between Precast Elements—Failure within Connection Region. *Journal of Structural Engineering*, V. 115, No. 12 (December): pp. 3171–3192.
7. Englekirk, R. 1995. Development and Testing of a Ductile Connector for Assembling Precast Concrete Beams and Columns. *PCI Journal*, V. 40, No. 2 (March–April): pp. 36–51.
8. Priestley, M. J. N., and G. A. MacRae. 1996. Seismic Tests of Precast Beam-to-Column Joint Subassemblages with Unbonded Tendons. *PCI Journal*, V. 41, No. 1 (January–February): pp. 64–80.
9. Ertas, O., S. Ozden, and T. Ozturan. 2006. Ductile Connections in Precast Concrete Moment Resisting Frames. *PCI Journal*, V. 51, No. 2 (May–June): pp. 2–12.
10. Soubra, K. S., J. K. Wight, and A. E. Naaman. 1993. Cyclic Response of Fibrous Cast-in-Place Connections in Precast Beam-Column Subassemblages. *ACI Structural Journal*, V. 90, No. 3 (May–June): pp. 316–323.
11. Restrepo, J. I., R. Park, and A. H. Buchanan. 1995. Tests on Connections of Earthquake Resisting Precast Reinforced Concrete Perimeter Frames of Buildings. *PCI Journal*, V. 40, No. 4 (July–August): pp. 44–61.
12. Lin, Z. F., E. I. Sagan, and M. E. Kreger. 1998. Study on the Ductile Connections for Precast Aseismic Frame. *Journal of Tongji University*, V. 26, No. 2 (April): pp. 135–138.
13. Priestley, M. J. N., S. Sritharan, J. R. Conley, and S. Pampanin. 1999. Preliminary Results and Conclusions from the PRESSS Five-Story Precast Concrete Test Building. *PCI Journal*, V. 44, No. 6 (November–December): pp. 42–67.
Rodriguez, M., and J. Blandon. 2005. Tests on a Half-Scale Two-Story Seismic-Resisting Precast Concrete Building. *PCI Journal*, V. 50, No. 1 (January–February): pp. 94–114.
14. Chinese Standard. 2001. *Code for Seismic Design of Buildings*. [In Chinese.] GB 50010-2001. Beijing, China: Chinese Building Press.
15. American Concrete Institute (ACI) Committee 318. 2008. *Building Code Requirements for Structural Concrete (ACI 318-08) and Commentary (ACI 318R-08)*. Farmington Hills, MI: ACI.
16. Park, R. 1989. Evaluation of Ductility of Structures and Structural Assemblages from Laboratory Testing. *Bulletin of the New Zealand National Society for Earthquake Engineering*, V. 22, No. 3 (September): pp. 55–166.
17. Kwak, H. G., and S. P. Kim. 2002. Cyclic Moment-Curvature Relationship of an RC Beam. *Magazine of Concrete Research*, V. 54, No. 6 (December): pp. 435–447.

Notation

- E_c = concrete elastic modulus
- E_s = steel elastic modulus
- f_{cu} = cube strength
- f_t = spilt strength
- f_u = ultimate strength
- f_y = yield strength
- F_1 = lateral load applied to first level of test structure
- F_2 = lateral load applied to second level of test structure
- h = beam depth
- K_{sec} = secant stiffness
- P = load
- P_{cr} = cracking load
- P_{max} = peak load
- P_y = yield load
- Δ_{cr} = displacement corresponding to cracking load
- Δ_{max} = displacement corresponding to maximum load
- Δ_u = ultimate displacement
- Δ_y = yield displacement

About the authors



Weichen Xue is a professor of structural engineering for the Department of Building Engineering at Tongji University in Shanghai, China. His research interests include precast, pre-stressed concrete structures;

composite structures; and fiber-reinforced polymer used in concrete structures.



Xinlei Yang is a PhD candidate for the College of Civil Engineering at Tongji University. His research interests include precast concrete structures and seismic design of reinforced concrete structures.

Synopsis

This paper presents the results of experimental investigations on four full-scale precast concrete connections and a half-scale, two-story, two-bay, precast concrete, moment-resisting frame, which consisted of composite concrete beams and cast-in-place concrete columns, under cyclic loading.

The precast concrete connections investigated in this paper included an exterior connection, an interior connection, a T connection, and a knee connection. Test results revealed that the four precast concrete connections, as expected, exhibited a strong column–weak beam failure mechanism and failed due to concrete crushing and fracturing of longitudinal bars as a result

of forming a plastic hinge at the fixed end of the beam.

The four connections behaved in a ductile manner. However, the displacement ductility of the knee connection was the poorest among them. The precast concrete frame exhibited a mixed side-sway mechanism and behaved in a ductile manner. The hysteresis curves of the frame were full and exhibited good energy-dissipation capacity. The global and interstory displacement ductility of the frame was not less than 4.5. In general, the seismic behavior of the precast concrete frame was satisfactory. This research could provide structural engineers with useful information about the safety of precast concrete–frame structures.

Keywords

Composite beam, connection, cyclic loading, ductility, energy dissipation, failure, frame, seismic, stiffness degradation.

Review policy

This paper was reviewed in accordance with the Precast/Prestressed Concrete Institute’s peer-review process.

Reader comments

Please address any reader comments to *PCI Journal* editor-in-chief Emily Lorenz at elorenz@pci.org or Precast/Prestressed Concrete Institute, c/o *PCI Journal*, 200 W. Adams St., Suite 2100, Chicago, IL 60606. 